



Article

Design of Low-Profile Single- and Dual-Band Antennas for IoT Applications

Wazie M. Abdulkawi , Abdel Fattah A. Sheta, Ibrahim Elshafiey and Majeed A. Alkanhal 

Department of Electrical Engineering, King Saud University, Riyadh 11421, Saudi Arabia; asheta@ksu.edu.sa (A.F.A.S.); ishafiey@ksu.edu.sa (I.E.); majeed@ksu.edu.sa (M.A.A.)

* Correspondence: walkadri@ksu.edu.sa

Abstract: This paper presents novel low-cost single- and dual-band microstrip patch antennas. The proposed antennas are realized on a square microstrip patch etched symmetrically with four slots. The antenna is designed to have low cost and reduced size to use in Internet of things (IoT) applications. The antennas provide a reconfigurable architecture that allows operation in different wireless communication bands. The proposed structure can be adjusted to operate either in single band or in dual-band operation. Two prototypes are implemented and evaluated. The first structure works at a single resonance frequency ($f_1 = 2.4$ GHz); however, the second configuration works at two resonance frequencies ($f_1 = 2.4$ GHz and $f_2 = 2.8$ GHz) within the same size. These antennas use a low-cost FR-4 dielectric substrate. The 2.4 GHz is allotted for the industrial, scientific, and medical (ISM) band, and the 2.8 GHz is allocated to verify the concept and can be adjusted to meet the user's requirements. The measurement of the fabricated antennas closely matches the simulated results.

Keywords: internet of things; microstrip antenna; slotted patch antenna; single-band; dual-band



Citation: Abdulkawi, W.M.; Sheta, A.F.A.; Elshafiey, I.; Alkanhal, M.A. Design of Low-Profile Single- and Dual-Band Antennas for IoT Applications. *Electronics* **2021**, *10*, 2766. <https://doi.org/10.3390/electronics10222766>

Academic Editor: Manuel Arrebola

Received: 20 October 2021

Accepted: 10 November 2021

Published: 12 November 2021

Publisher's Note: MDPI stays neutral with regard to jurisdictional claims in published maps and institutional affiliations.



Copyright: © 2021 by the authors. Licensee MDPI, Basel, Switzerland. This article is an open access article distributed under the terms and conditions of the Creative Commons Attribution (CC BY) license (<https://creativecommons.org/licenses/by/4.0/>).

1. Introduction

Lately, technology growth has been increasing rapidly. Most things in the world and human life will be affected by the Internet. Therefore, the Internet of things (IoT) received extensive consideration in observing and sensing applications [1,2]. The IoT consists of the observation region for sensing data, network region for transmitting data, and application region for connecting the objects and the cloud network. In the IoT, numeral devices, sensors, equipment, and things communicate with others through the cloud network [3]. Many antenna configuration types for IoT applications have been presented in recent years [4–6].

Single-band antennas can be used in some general equipment. However, modern systems need multi-functionally and smart antennas, which demonstrate higher efficiency and are compact. As technology rapidly grows, modern wireless systems (IoT devices) exhibit various functions and require operation at more than one frequency without increasing the antenna size [7–10]. In the literature, different shapes of the single-band and multi-band monopole antennas have been developed, such as H-shaped [11], circular-shaped [12], U-shaped open stub [13], M-shaped open stub [14], L-shape with coupled branch strip [9], L-shaped stub folded into U-shaped [4], D-shaped [15], U-shaped with rectangular patch inside [16], square spiral loop [17], tapered rectangular patch antenna [5], and symmetric bow-tie circular patch antenna [18]. Dual-band or multi-band operations can be obtained by etching some slots either in the radiating elements [3,18–22], in the ground plane of the antennas [23–26], or both [9,27,28]. A square microstrip patch etched with four symmetrical slots [29–33] has been proposed for nondegenerate dual-mode filter applications.

Table 1 shows the performance comparison for previously published single-, dual-, and multi-band antennas. In this table, three of the proposed structures with good performance are included.

Table 1. Comparison of the proposed antenna with another state-of-the-art.

Ref.	Antenna Type	Substrate	No. of Ports	Resonance Frequencies (GHz)	Dimensions (mm ²)	Maximum Gain (dB)	Bandwidth (MHz)
[1]	Slotted patch	FR-4	2	1.73 and 2.53	48 × 48	−3.8 and 1.9	30
[4]	U-shaped	Rogers RO4003	1	3.5	14 × 14	1.42	200
[5]	Slotted patch	FR-4	5	0.9, 1, 1.72, 2.18, 5 and 5.5	120 × 65	0.53, −0.96, 1.97, 3.75, 2.46, and 4.9	150
[6]	PIFA	FR-4	1	1.8 and 2.4	45 × 32	1.6 and 1.8	50
[11]	H-shaped	Rogers RT5880	1	1.8	72 × 17	5.5	40
[12]	Slotted circular patch	FR-4	1	1.8	24 × 40	1.9	180
[34]	Meander line	FR-4	1	2.4	40 × 10	1.35	146
[35]	Slotted	FR-4	1	2.4, 3.5, and 5.8	80 × 80	2.33, 3.14, and 2.89	140
[36]	C-shaped	FR-4	1	1.8, 2.4, and 5	209 × 260	4.40, 4.75, and 5.25	100
[15]	Monopole	FR-4	1	2.4 and 5	34 × 26	2.2 and 2	220
This work	Slotted square	Rogers RT5880	1	2.4	41.5 × 38.5	3.39	18
	Wideband slotted square	FR-4		2.4 and 2.8	38.5 × 38.5	3.45 and 3.2	20
				2.4	36.4 × 36.4	2.45	220

This study proposes a slotted square patch antenna for IoT applications. The antenna is designed to have low cost and reduced size to allow use in IoT applications. The antenna provides a reconfigurable architecture that allows operation in receive or transmit modes at the specified frequency. In addition, the antenna can be used in a full-duplex system transmitting and receiving at different frequencies. This study can reduce the interference with other nodes in the IoT network. The proposed antenna can operate at dual resonant frequencies. Two prototypes are designed and fabricated on low-cost FR-4 substrate ($\epsilon_r = 4.3$, $\tan \sigma = 0.025$, and $h = 1.6$ mm). The first configuration works at a single resonance frequency ($f_1 = 2.4$ GHz); however, the second configuration was developed to work at two resonance frequencies ($f_1 = 2.4$ GHz and $f_2 = 2.8$ GHz) within the same size. The two prototypes are fabricated, and the results are validated. The measured results correlate well with the simulated one.

The study is scheduled as follows. The non-slotted and slotted square patch antennas are discussed in Sections 2 and 3, respectively. In Section 4, the single-band antenna is designed and explained. The dual-band antenna is discussed in Section 5. In Section 6, the bandwidth improvement is discussed. Section 7 displays the simulated and measured results for both antennas. The conclusion and discussions are presented in Section 8.

2. Non-Slotted Square Patch

The square patch resonator can be considered as a square cavity with magnetic walls. The field inside the square cavity matches those of TM_{mn0}^z modes [37]. The consequential modes of the square patch type (TM_{mn0}^z) can be calculated using the same method as described in [29]. The resonance frequencies of the resultant modes for the non-slotted square patch can be obtained using [38]:

$$f_{m,n} = \frac{150}{\alpha \sqrt{\epsilon_{eff}}} \sqrt{m^2 + n^2} \text{ GHz}, \quad (1)$$

where m and n are the nonnegative integer numbers and the effective relative permittivity (ϵ_{eff}) is given using

$$\epsilon_{eff} = \begin{cases} \epsilon_{eff}(w) & \text{if } m = 0 \\ \epsilon_{eff}(w) & \text{if } n = 0 \\ \frac{\epsilon_{eff}^2(w)}{\epsilon_r} & \text{otherwise} \end{cases} \quad (2)$$

$$\epsilon_{eff}(w) = \frac{1}{2} \left(\epsilon_r + 1 + \frac{(\epsilon_r - 1)}{\sqrt{1 + \frac{10h}{w}}} \right) \quad (3)$$

where w is the square width in mm, and α is the effective width of the square, given as:

$$\alpha = w + 2|\Delta w| \text{ mm} \quad (4)$$

$$\Delta w = 0.412h \frac{\epsilon_{eff}(w) + \left(\frac{0.3w}{h}\right) + 0.264}{\epsilon_{eff}(w) - \left(\frac{0.258w}{h}\right) + 0.8}, \quad (5)$$

where h is the substrate thickness in mm.

The performance of a microstrip antenna is affected by fringing fields. The strength of the fringing field is mainly dependent on the patch's dimensions and the substrate's height. Due to the fringing field, the physical dimensions of the square patch appear smaller than its effective electrical dimensions [39]. Because of the fringing field, the effective width (α) increased by $2\Delta w$.

In our design, the 20 mm long non-slotted square patch is designed on the top of the low-cost FR-4 substrate with relative permittivity ($\epsilon_r = 4.3$) and thickness of $h = 1.6$ mm. Here, the resonance frequencies of the first two fundamental modes (degenerate modes), TM_{100} and TM_{010} , are equal ($f_{100} = f_{010} = 2.805$ GHz). For the TM_{110} mode, the resonance frequency is $f_{110} = 3.966$ GHz. Modes' resonance frequencies depend on the current distribution of each mode. As an example, the current parallel to the X-direction excites only the TM_{100} mode, the current parallel to Y-direction excites only the TM_{010} mode, and the current parallel to the diagonal excites the three modes. The feeding mechanism mainly determines the current in the patch. Therefore, appropriate feeding can control the excited modes and thus the resonance frequencies of the patch. The symmetric feed lines are used to excite the single dominant mode; however, asymmetrical feed lines are used to excite the two degenerate modes [29]. In addition to that, differential excitation is used to excite the modes, such as the TM_{10} and TM_{30} modes for rectangular patch [40,41], and TM_{10} and TM_{11} modes for an equilateral triangular microstrip patch antenna [42].

3. Slotted Square Patch

Figure 1 illustrates the geometry of the proposed slotted square patch antenna. The main building block of the proposed antenna is a microstrip square patch with length L . The square patch is etched with four symmetrical slots along X- and Y-axes, as shown in the figure. All slots have the same length (L_s) and width (W_s).

For the slotted square patch in Figure 1, the vertical slots (along the Y-axis) cut the current parallel to the X-axis and increase the effective length of the TM_{100} mode and decrease its resonance frequency. Similarly, the horizontal slots cut the contemporary parallel to the Y-axis and increase the effective length of the TM_{010} mode that reduces its resonance frequency. For symmetrical slots, both the TM_{100} and TM_{010} are affected simultaneously in the same manner, and therefore they have the same resonance frequency denoted f_1 . The resonance frequencies of these two modes decrease as the lengths of the slots L_s increase. These two modes can be excited simultaneously, or only one of them can be excited according to the feeding mechanism. The vertical and horizontal slots cut the current of the TM_{110} mode, and thus, its resonance frequency, denoted as f_2 , decreases

faster with the lengths of the slots L_s . The slots' resultant modes can be considered distorted types of those described in the above section. The effect of the length of the slot L_s and width W_s on the resonance frequencies of the modes TM_{100} , TM_{010} , and TM_{110} , is studied using the patch of side $L = 20$ mm on low-cost FR-4 substrate with $\epsilon_r = 4.3$, thickness $h = 1.6$ mm, and loss tangent of 0.025. The resonance frequencies f_1 and f_2 generated by computer simulation technology (CST) simulators using the same technique presented in [29] are shown in Figure 2. The resonance frequencies f_1 and f_2 decrease as the slots' L_s lengths increase, but f_2 decreases faster since it is affected by both vertical and horizontal slots. It has to be shown that these frequencies are also affected by the width of the slots, and this can be used to add more fine control of the resonance frequencies of each mode, as will be seen in the next section. Figure 2 can be generated for any other patch length L and any other dielectric material.

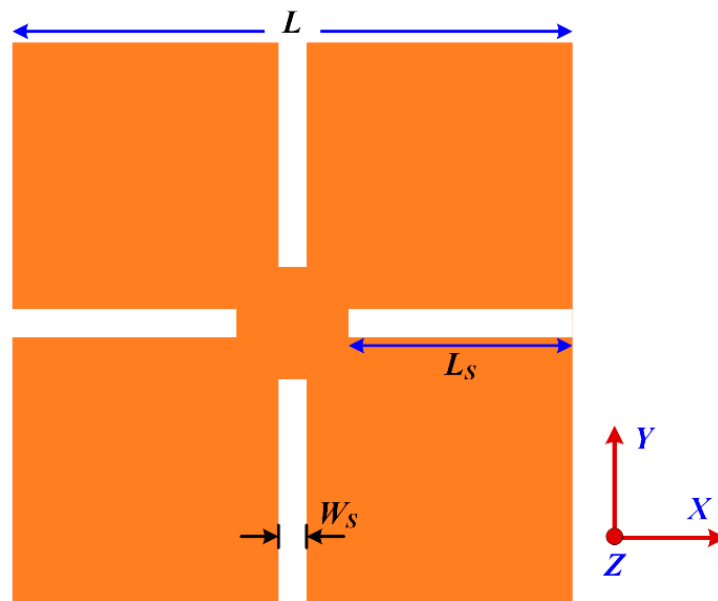


Figure 1. The geometry of the proposed slotted square patch ($L = 20$ mm).

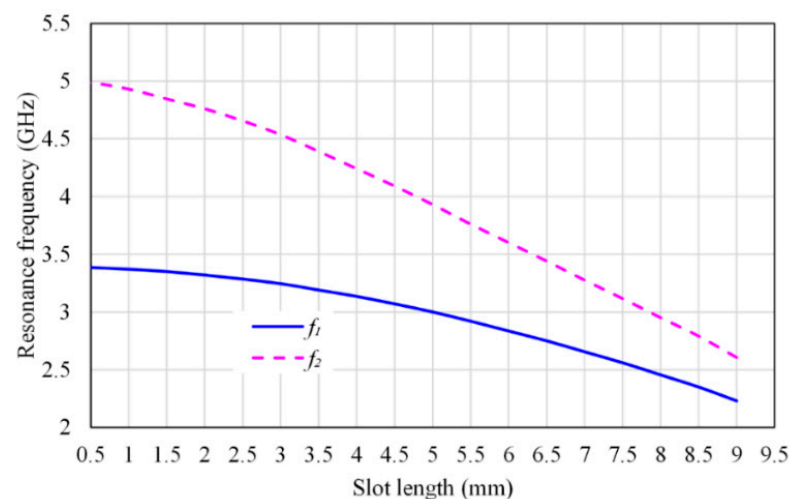


Figure 2. Resonance frequencies (f_1 and f_2) variations with L_s at $W_s = 1$ mm.

4. Single-Band Antenna Design

The same patch size of length $L = 20$ mm is considered in this design. Only one of the two modes, TM_{100} and TM_{010} , can be excited by the inset feed. The TM_{100} mode is the only exciting mode if the feeder is positioned along the X-axis as shown in Figure 3. The

width of the feed line can be optimized for matching purposes. The single band operation at the specific frequency of this antenna can be adjusted by the appropriate selection of the slot's length and width. The characteristics of the designed antenna were simulated and calculated using a CST simulator. Figure 4a,b shows the effect of the dimensions of the slot on S_{11} performance of the antenna. First, Figure 4a shows the result of the L_S variation on the resonance frequency f_1 when the slot width is 1 mm.

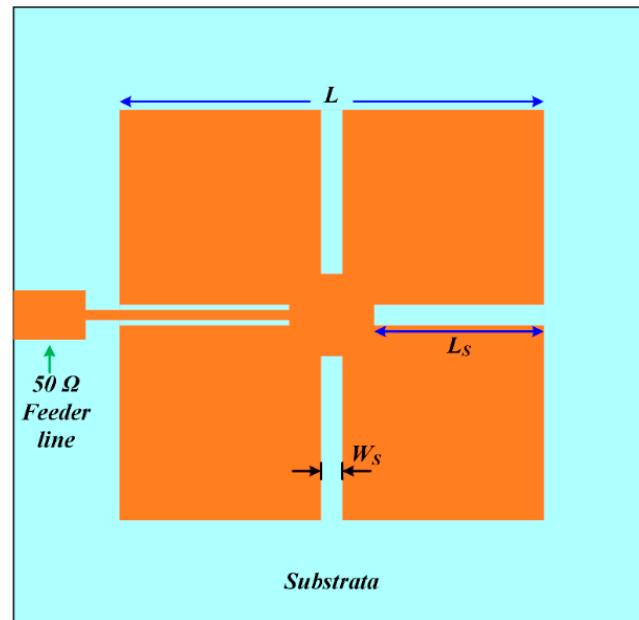


Figure 3. The slotted antenna with inset fed along the X-axis.

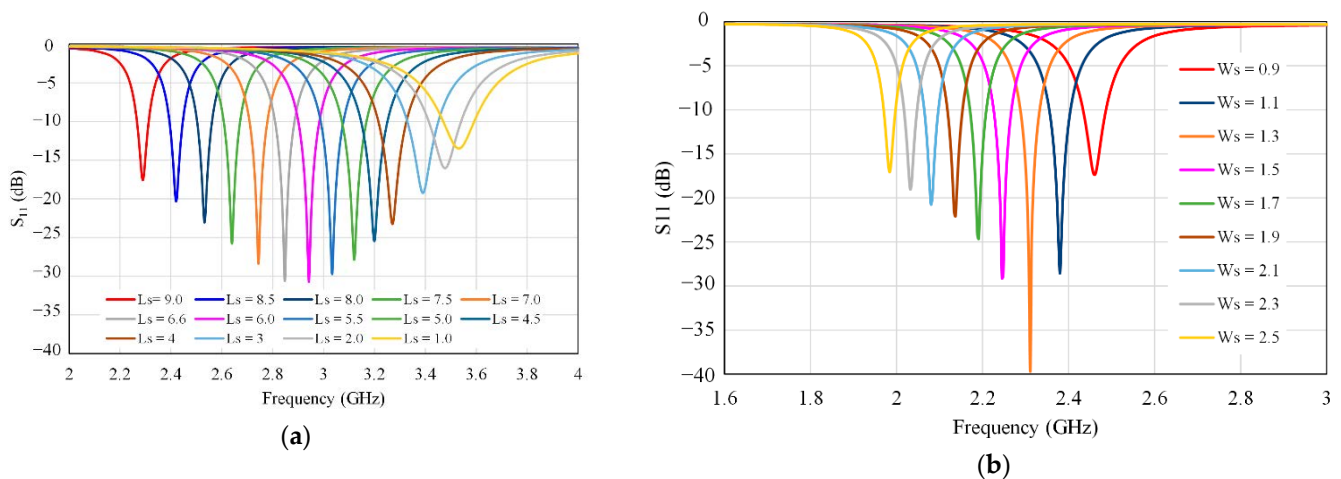


Figure 4. Frequency responses of slotted square patch antenna (single-band) (a) for different L_S values, with $W_S = 1$ mm, and (b) for different W_S values, with $L_S = 8.5$ mm.

As slot length increases, the resonance frequency f_1 decreases. The effect of slots width W_S on the resonance frequency f_1 is observed in Figure 4b for slot length = 8.5 mm. The slot's width can be used for fine adjustment of f_1 . As slot width increases, the resonance frequency f_1 decreases.

The single band antenna design is selected to operate at 2.4 GHz, corresponding to slot length 8.5 mm and width 1 mm. The simulated S_{11} is shown in Figure 5.

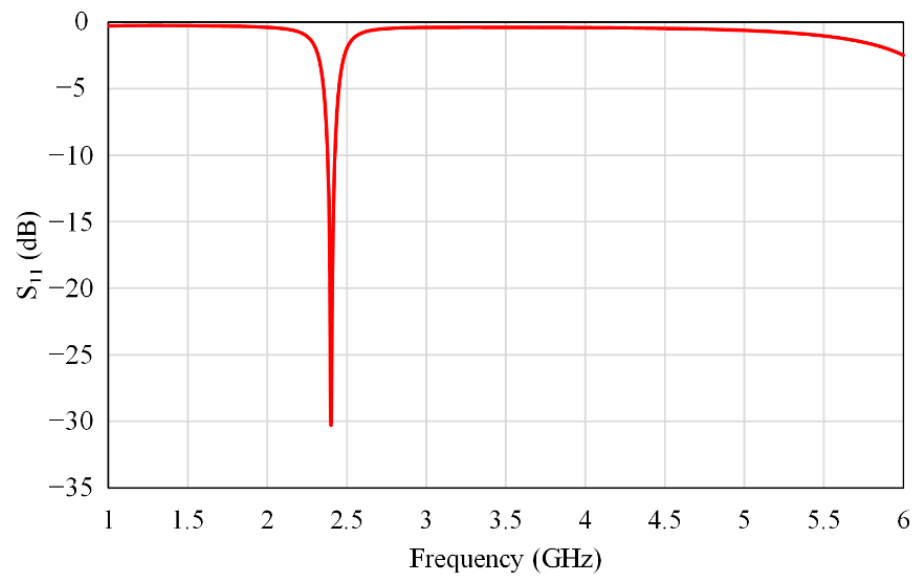


Figure 5. Simulated return loss (S_{11}) of the single-band slotted square antenna.

Figure 6 shows the surface current distribution for the developed single-band antenna at 2.4 GHz. It is observed from this figure that the current along the X-axis turned around the vertical slots and increased the effective length of the patch.

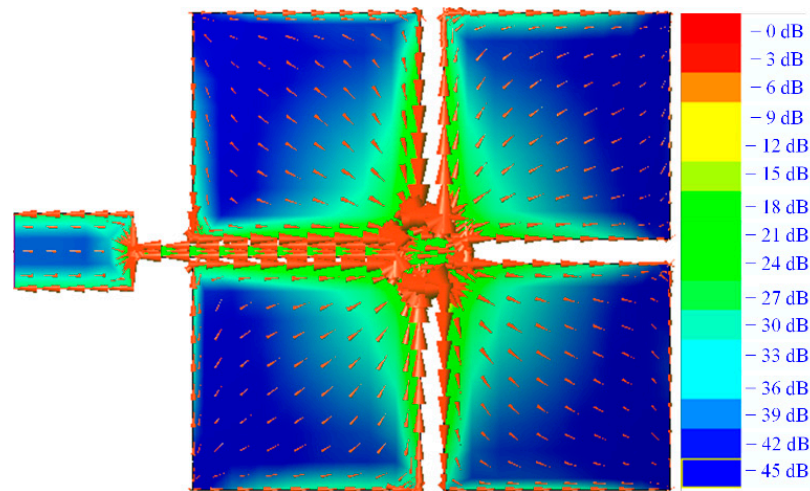


Figure 6. Current distribution for single-band slotted square patch antenna at 2.4 GHz.

In addition, the simulated 2D and 3D radiation patterns at 2.4 GHz are shown in Figure 7. It has been noted that the proposed antenna gain with FR-4 substrate is less than 0 dB, while the directivity = 4.72 dB. This gain reduction is due to the low performance of the low-cost FR-4 substrate. The low gain can be overcome using high-quality dielectric material such as RT Duroid 5880. Another antenna is designed on this substrate with the parameters: $\epsilon_r = 2.2$, thickness = 1.6 mm, and loss tangent = 0.0009 to prove the concept. The patch dimensions are optimized to operate at the same 2.4 GHz frequency as: patch length = 24 mm, slot length = 9.4 mm, and slot width = 4.5 mm. A little increase in the patch length is observed due to the decrease in the dielectric constant. The simulated S_{11} and 2D radiation patterns of this antenna are shown in Figure 8. A significant increase of 3.95 dB in the gain is observed.

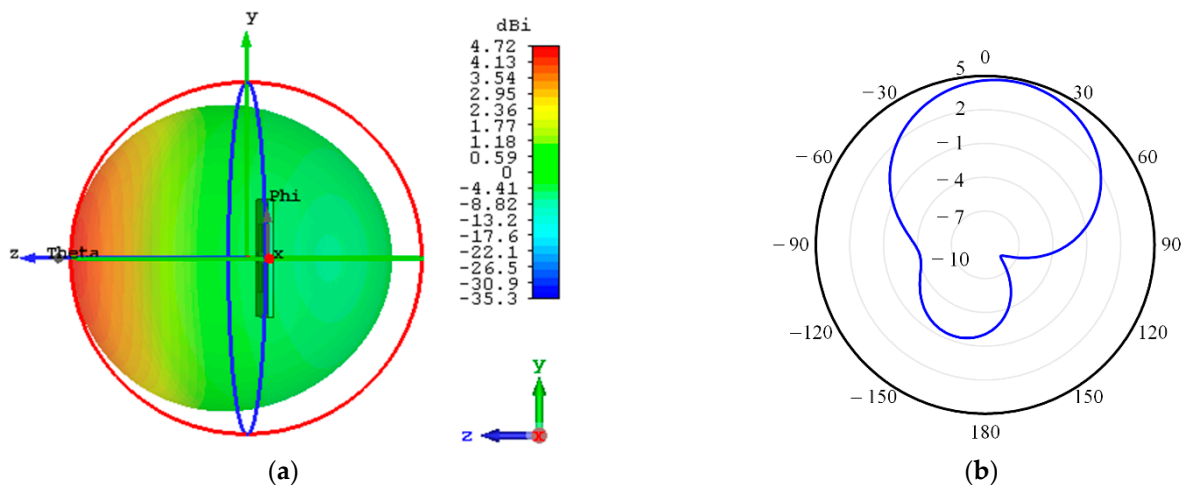


Figure 7. The simulated directivity of the proposed antenna with FR-4 substrate at 2.4 GHz (a) 3D and (b) 2D.

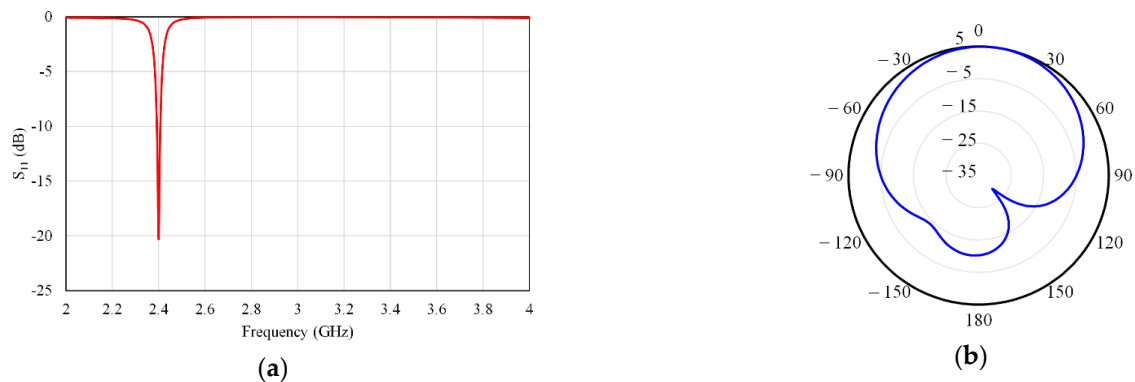


Figure 8. (a) The simulated results of the proposed antenna with RT-Duroid 5880 substrate at 2.4 GHz (a) S_{11} response and (b) 2D radiation pattern.

5. Dual-Band Antenna Design

Figure 9 shows the dual-mode slotted patch antenna with a coaxial probe feeder. By using this feeding technique, the three modes are excited. The degenerate modes TM_{100} and TM_{010} have the same resonance frequency f_1 , and the TM_{110} mode has resonance frequency f_2 . The probe position is selected by trials to match all modes. The dual-frequency of operation can be chosen directly from Figure 2 at a specific slot length when the width of the slot is 1 mm. More analysis can also be added for more design flexibility. Figure 10a,b shows the effect of the dimensions of the slot on S_{11} performance of the dual-band antenna. Figure 10a shows the effect of L_s for constant $W_s = 1$ mm, and Figure 10b illustrates the effect of W_s for $L_s = 8.5$ mm. The slot's width can be used for fine adjustment of f_1 and f_2 . As the slot width increases, the resonance frequencies f_1 and f_2 decrease.

The dual-band antenna design is selected to operate at 2.4 GHz and 2.8 GHz, corresponding to slot length 8.5 mm and width 1 mm. Figure 11 shows the simulated S_{11} of the proposed dual-band antenna.

Figure 12a,b shows the current distribution at these two resonance frequencies, respectively. It is observed from the distributions that the vertical and horizontal slots will affect the resonance frequency of the TM_{100} and TM_{010} modes, respectively. However, the TM_{110} mode has currents in both X and Y directions. Thus, its resonance frequency will be affected by both vertical and horizontal slots. Figure 13 shows the 3D radiation pattern at f_1 and f_2 . The gain of the proposed dual-band antenna with FR-4 substrate is still less than 0 dB. This issue is due to the low performance of the low-cost FR-4 substrate. However, the gain can be improved by using any other high-performance substrate. For example, the

simulation of the same dual-band antenna with RT Duroid 5880 substrate shows that the gain can be increased to about 3.45 dB and 3.2 dB at 2.4 GHz and 2.8 GHz, respectively. The radiation patterns of the dual-band slotted square patch antenna are shown in Figure 14. It is observed that a maximum gain of 3.45 dB (at 2.4 GHz) and 3.2 dB (at 2.8 GHz) are in the broadside direction.

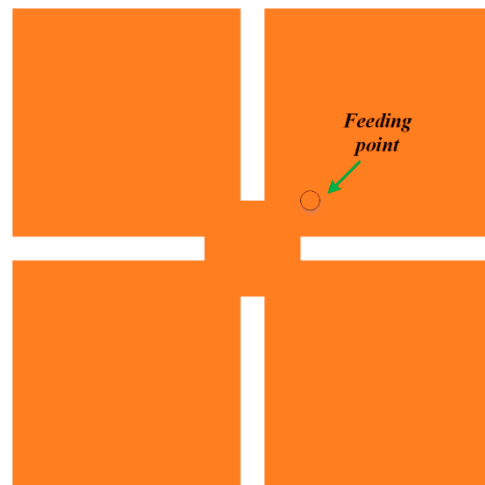


Figure 9. Dual-band antenna geometry.

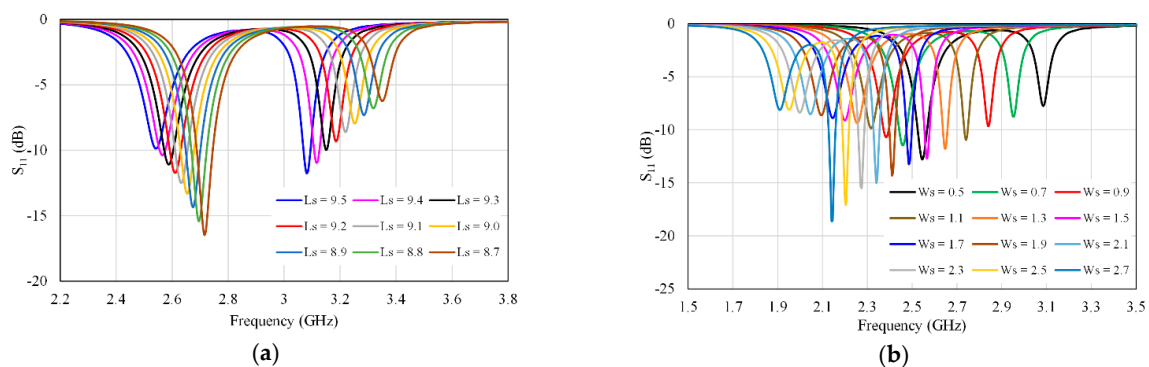


Figure 10. Frequency responses of slotted square patch antenna (dual-band) (a) for different L_s values, with $W_s = 0.2$ mm, and (b) for different W_s values, with $L_s = 8.5$ mm.

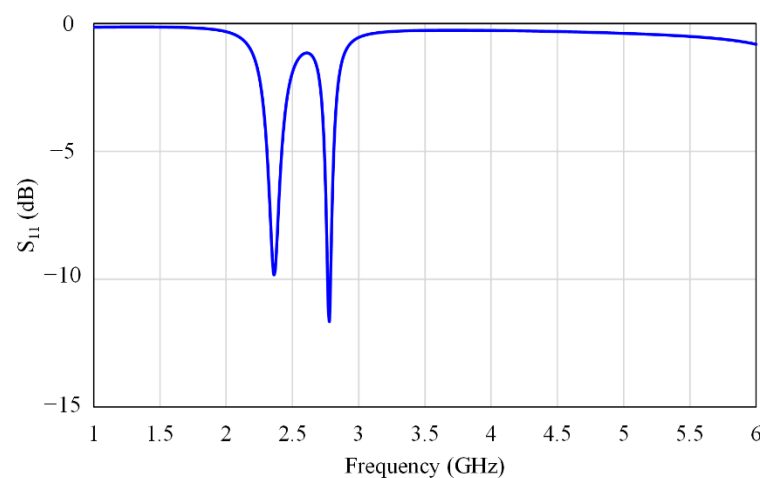


Figure 11. Simulated S_{11} for slotted patch antenna.

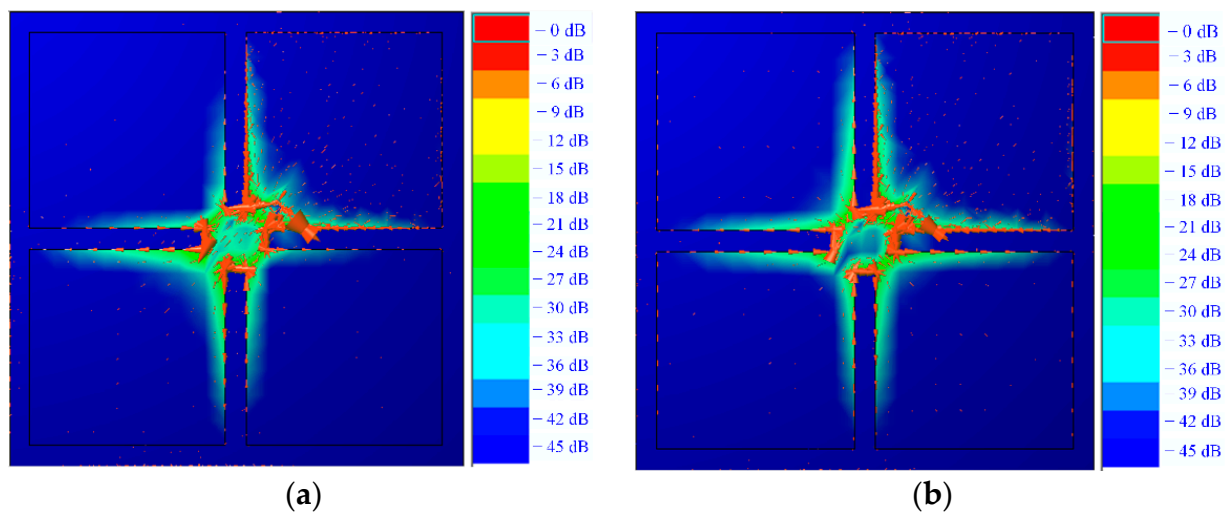


Figure 12. Current distribution for dual-band slotted square patch antenna at (a) 2.4 GHz and (b) 2.8 GHz.

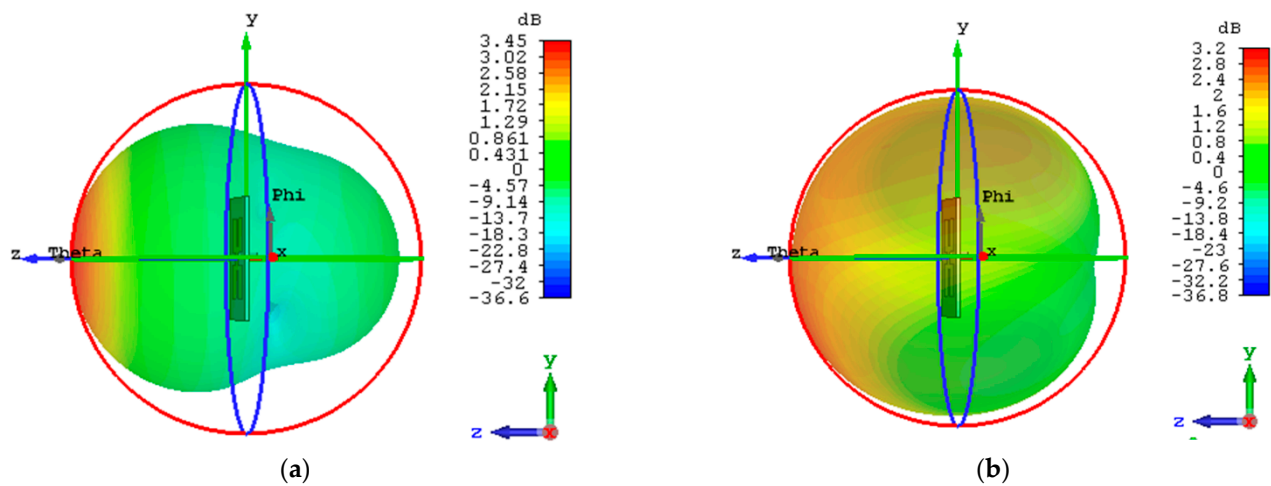


Figure 13. 3D radiation patterns of the dual-band slotted square patch antenna at (a) 2.4 GHz and (b) 2.8 GHz.

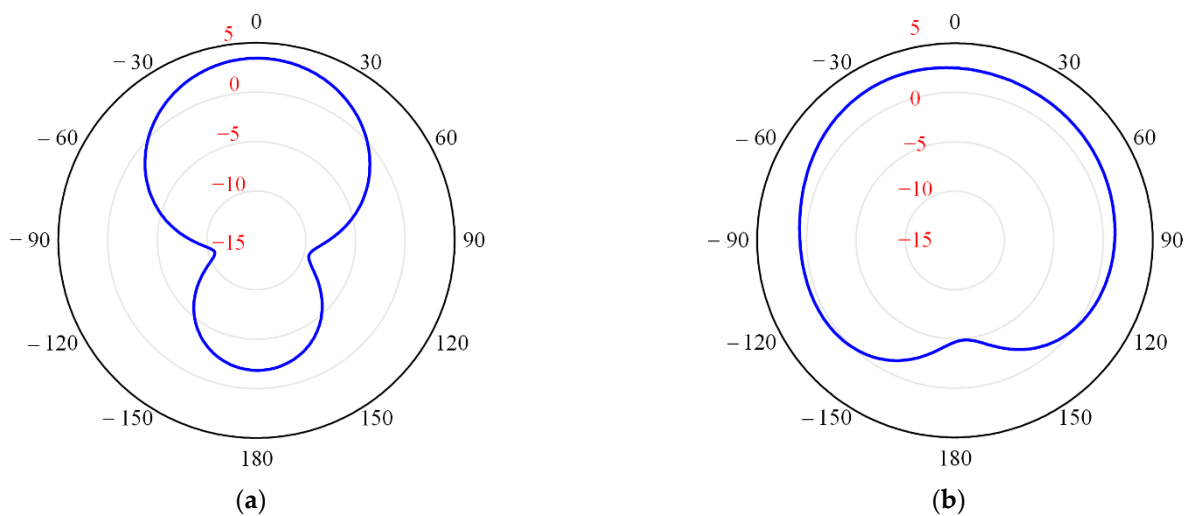


Figure 14. 2D radiation patterns of the dual-band slotted square patch antenna at (a) 2.4 GHz and (b) 2.8 GHz.

6. Bandwidth Enhancement

Conventional microstrip antenna structures are narrowband and their impedance bandwidth is typically 1–2%. However, the bandwidth can be improved by either increasing the substrate thickness, decreasing the dielectric constant (ϵ_r) of the substrate [43–47], or both. Other techniques, such as proximity coupled feed [48], aperture-coupled feed [49,50], and L-shaped feeding probe [51,52], can also be used. Some other configurations are suggested, such as slotted antenna [53,54], log-periodic array [55], E-shaped patch [56], circularly polarized patches [57,58], and defected ground method [59,60].

In this paper, bandwidth enhancement is attained for the same proposed structure by increasing the substrate thickness and decreasing the dielectric constant (ϵ_r). This arrangement is developed by adding foam substrate between the ground and the upper FR-4 substrate. For the matching purpose, a slot of size $6 \times 6 \text{ mm}^2$ is etched at the center of the radiating patch. The modified structure is shown in Figure 15. Figure 16 shows the simulated S_{11} of the modified structure. As observed from this figure, significant bandwidth improvements with -10 dB bandwidth of 220 MHz (2.33–2.54 GHz) are achieved.

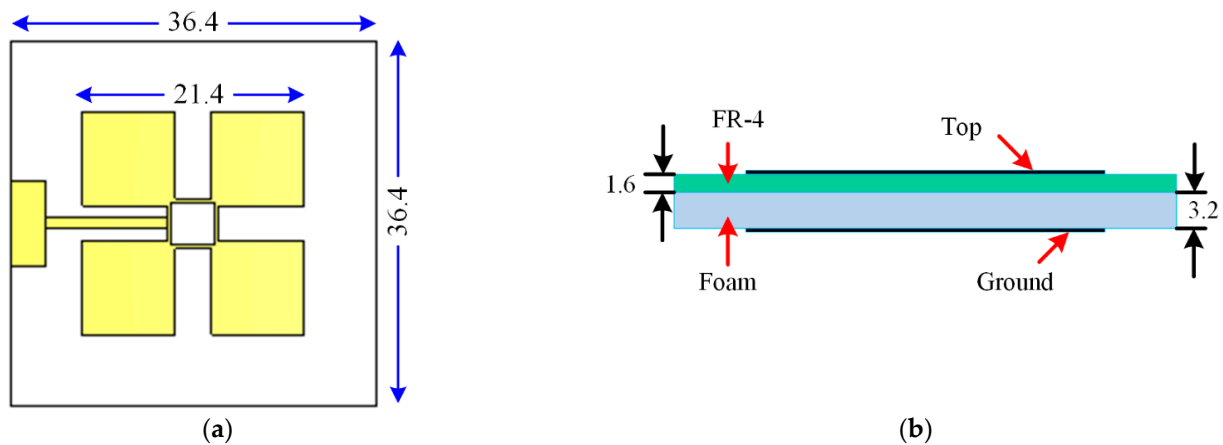


Figure 15. The modified single band antenna (a) top view and (b) side view (units: mm).

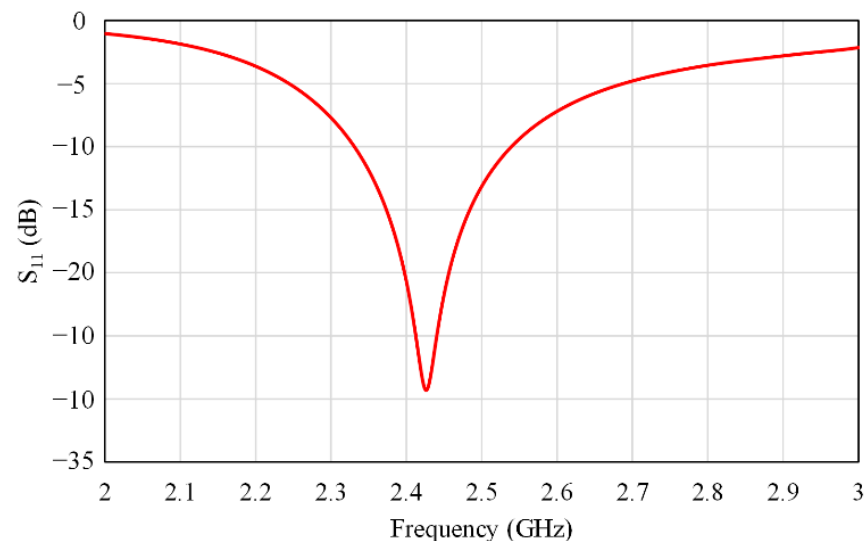


Figure 16. The simulated S_{11} of the modified single band antenna.

The simulation of this structure shows a significant increase in the gain of the antenna. The maximum gain of the antenna with FR-4 is less than 0 dB, while this structure gain is increased to 1.87 dB.

7. Experimental Results

Two prototypes for this antenna are fabricated and evaluated: one for a single-fed single-band antenna and the other for a single-fed dual-band antenna. Figure 17 shows photographs of the fabricated slotted square patch antennas. Both antennas are designed and simulated using CST simulators. However, experimental validation was conducted using the Anritsu Vector Network Analyzer (Anritsu VNA 37369C). Figure 18 shows the simulated and measured S_{11} for the fabricated single-band antenna. Further, Figure 19 shows the comparison between the simulated and measured S_{11} for the dual-band antenna. The figures show that the simulation and measured results closely match.

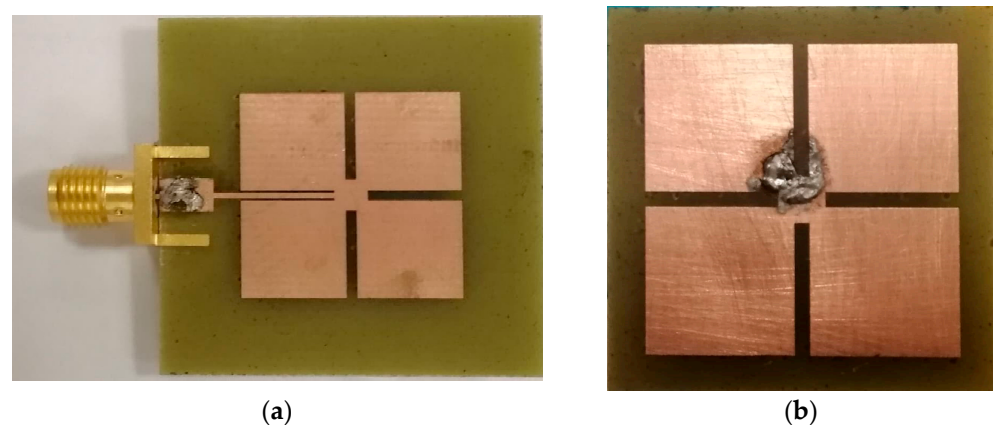


Figure 17. Photographs of the slotted square patch antenna in the (a) single-band and (b) dual-band.

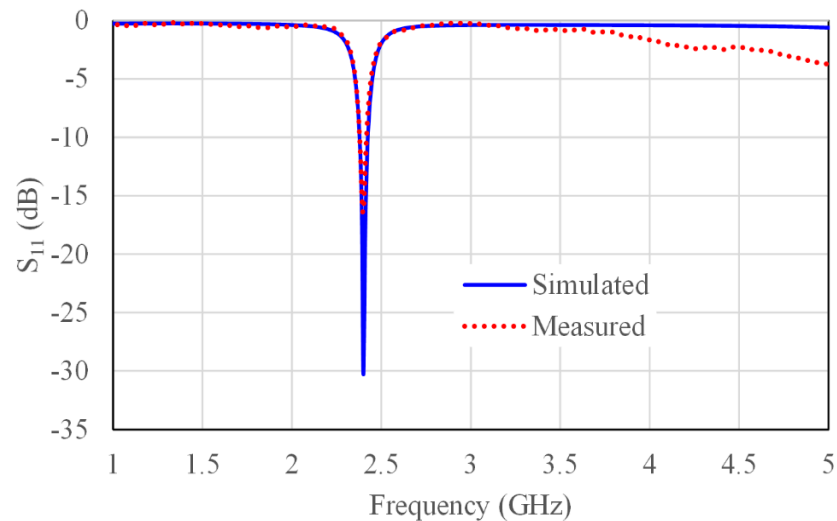


Figure 18. Simulated and measured return loss (S_{11}) of the single-fed single-band slotted square antenna.

In addition, a time-domain antenna measurement system GEOZONDAS (GEOZONDAS-TDAMS) [61] is used to measure the radiation patterns for the proposed antenna. A measurement setup was established to validate the far-field radiation pattern of the antenna, as shown in Figure 20. The antenna under test was placed on the top of the rotor, as shown in Figure 21. Figures 22 and 23 illustrate the simulated and measured radiation patterns of the single band antenna on xz-plane with FR-4 substrate and RT Duroid 5880 substrate, respectively.

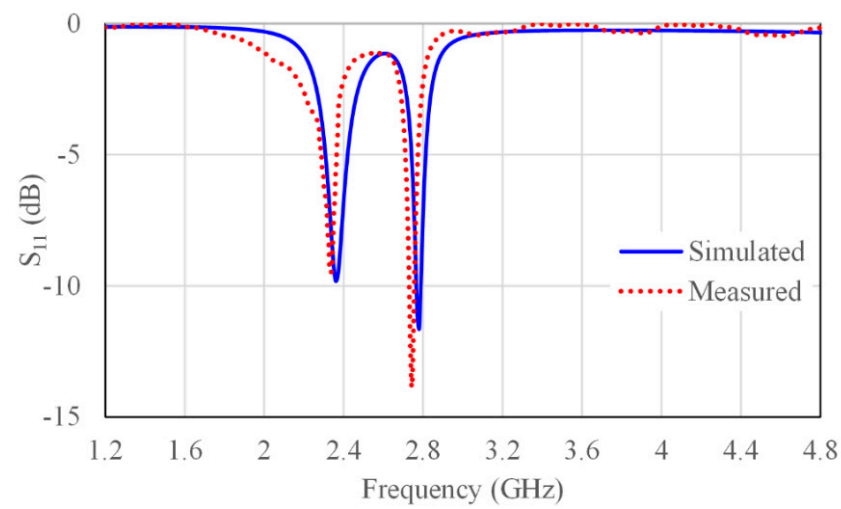


Figure 19. Simulated and measured return loss (S_{11}) of the single-fed dual-band slotted square antenna.

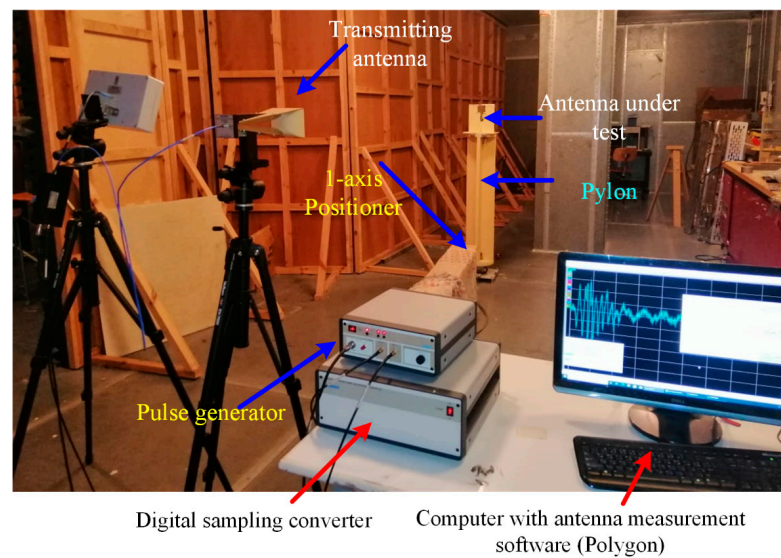


Figure 20. The measurement setup of the antenna radiation pattern.

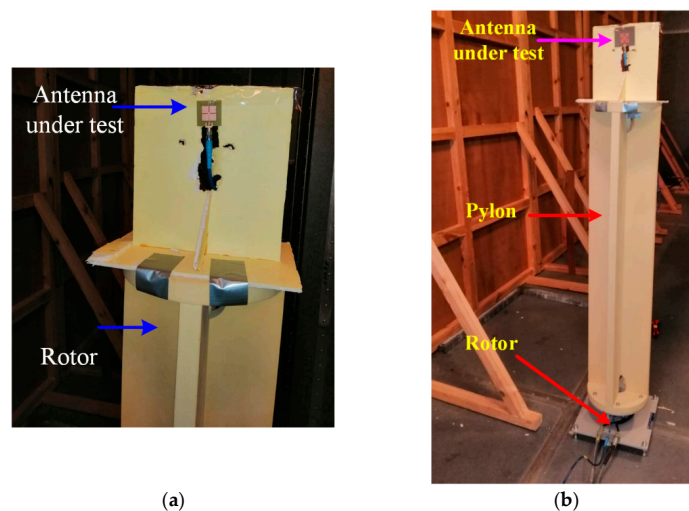


Figure 21. The antenna under test with (a) FR-4 substrate and (b) RT Duroid 5880 substrate.

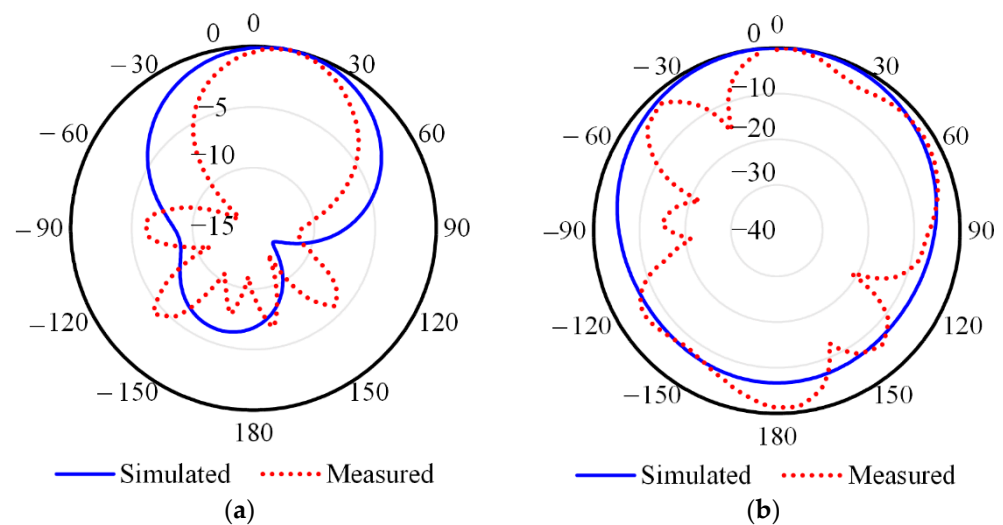


Figure 22. The simulated and measured radiation pattern of the single band antenna (using low-cost FR-4 substrate) at 2.4 GHz on (a) E-plane and (b) H-plane.

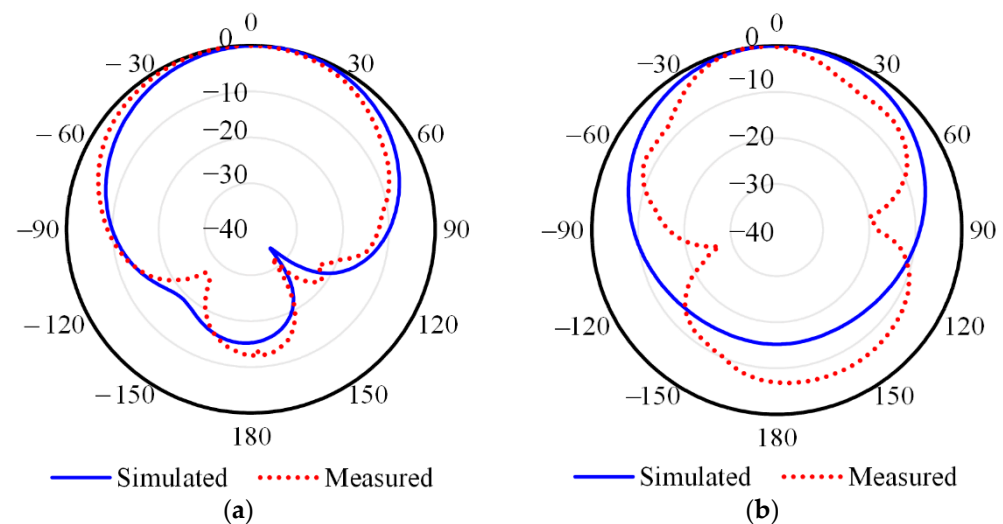


Figure 23. The simulated and measured radiation pattern of the single band antenna (using RT Duroid substrate) at 2.4 GHz on (a) E-plane and (b) H-plane.

8. Conclusions

This study demonstrated a novel single-fed single-band and dual-band microstrip patch antenna. This antenna was realized on a square microstrip patch etched symmetrically with four slots. The antenna was designed to have low cost and reduced size to allow use in IoT applications. This antenna provides a reconfigurable architecture that allows operation in receive or transmit modes at the specified frequency. In addition, the antenna can be used in a full-duplex system sending and receiving at different frequencies, which can reduce the interference with other nodes in the IoT network. The proposed antenna operates at dual operating frequency bands of 2.4 GHz and 2.8 GHz that have been specified for the upcoming IoT technology. Two prototypes were fabricated with low-cost FR-4 substrate and tested. The first antenna works at a single resonance frequency ($f_1 = 2.4$ GHz); however, the second structure works at two resonance frequencies ($f_1 = 2.4$ GHz and $f_2 = 2.8$ GHz) within the same size. The 2.4 GHz is allotted for the industrial, scientific, and medical (ISM) band, and the 2.8 GHz is allocated to verify the concept and can be adjusted to meet the user's requirements. The results were successfully demonstrated regarding return loss, radiation, and gain. The maximum gain achieved by

the dual-band antenna is 3.45 dB and 3.2 dB at 2.4 GHz and 2.8 GHz, respectively. The measurement of the fabricated antennas closely matched the simulated results.

Author Contributions: Conceptualization, A.F.A.S. and M.A.A.; methodology, W.M.A., A.F.A.S., I.E. and M.A.A.; software, W.M.A.; validation, W.M.A.; formal analysis, W.M.A., A.F.A.S., I.E. and M.A.A.; investigation, A.F.A.S., I.E. and M.A.A.; resources, A.F.A.S., I.E. and M.A.A.; data curation, W.M.A.; writing—original draft preparation, W.M.A.; writing—review and editing, W.M.A., A.F.A.S., I.E. and M.A.A.; visualization, W.M.A. and A.F.A.S.; supervision, A.F.A.S., I.E. and M.A.A.; project administration, A.F.A.S.; funding acquisition, A.F.A.S. All authors have read and agreed to the published version of the manuscript.

Funding: This research received no external funding.

Institutional Review Board Statement: Not applicable.

Informed Consent Statement: Not applicable.

Data Availability Statement: Not applicable.

Acknowledgments: This project was funded by the National Plan for Science, Technology, and Innovation (MAARIFAH), King Abdulaziz City for Science and Technology, Kingdom of Saudi Arabia, Award Number (15-ELE5017-02).

Conflicts of Interest: The authors declare no conflict of interest.

References

1. Wang, M.; Yang, L.; Shi, Y. A Dual-port Microstrip Rectenna for Wireless Energy Harvest at LTE Band. *AEU Int. J. Electron. Commun.* **2020**, *126*, 153451. [\[CrossRef\]](#)
2. Kumar, N.; Khanna, R. A compact multi-band multi-input multi-output antenna for 4G/5G and IoT devices using theory of characteristic modes. *Int. J. RF Microw. Comput. Aided Eng.* **2020**, *30*, e22012. [\[CrossRef\]](#)
3. Goswami, P.K.; Goswami, G. Truncated T parasite staircase fractal U-slot antenna for multiple advance internet of things applications. *Microw. Opt. Technol. Lett.* **2020**, *62*, 830–838. [\[CrossRef\]](#)
4. Mao, Y.; Guo, S.; Chen, M. Compact dual-band monopole antenna with defected ground plane for Internet of things. *IET Microw. Antennas Propag.* **2018**, *12*, 1332–1338. [\[CrossRef\]](#)
5. Jha, K.R.; Bukhari, B.; Singh, C.; Mishra, G.; Sharma, S.K. Compact Planar Multistandard MIMO Antenna for IoT Applications. *IEEE Trans. Antennas Propag.* **2018**, *66*, 3327–3336. [\[CrossRef\]](#)
6. Chen, L.; Zhang, H.; Chen, Z.; Zhang, Y.; Yao, J.; Xing, Y. Design of Low-profile Dual-band Antenna for IoT Applications. In Proceedings of the 2019 3rd International Conference on Electronic Information Technology and Computer Engineering (EITCE), Xiamen, China, 18–20 October 2019; pp. 1805–1809.
7. Chen, S.; Dong, D.; Liao, Z.; Cai, Q.; Liu, G. Compact wideband and dual-band antenna for TD-LTE and WLAN applications. *Electron. Lett.* **2014**, *50*, 1111–1112. [\[CrossRef\]](#)
8. Lee, H.; Ren, D.; Choi, J.H. Dual-Band and Polarization-Flexible CRLH Substrate-Integrated Waveguide Resonant Antenna. *IEEE Antennas Wirel. Propag. Lett.* **2018**, *17*, 1469–1472. [\[CrossRef\]](#)
9. Chung, M.-A. A miniaturized triple band monopole antenna with a coupled branch strip for bandwidth enhancement for IoT applications. *Microw. Opt. Technol. Lett.* **2018**, *60*, 2336–2342. [\[CrossRef\]](#)
10. Abdulkawi, W.; Malik, W.; Rehman, S.; Aziz, A.; Sheta, A.; Alkanhal, M. Design of a Compact Dual-Band MIMO Antenna System with High-Diversity Gain Performance in Both Frequency Bands. *Micromachines* **2021**, *12*, 383. [\[CrossRef\]](#) [\[PubMed\]](#)
11. Abdulkawi, W.M.; Sheta, A.-F.A.; Malik, W.A.; Rehman, S.U.; Alkanhal, M.S. RF MEMS Switches Enabled H-Shaped Beam Reconfigurable Antenna. *Appl. Comput. Electromagn. Soc. J.* **2019**, *34*, 1312–1319.
12. Abdulkawi, W.M.; Malik, W.A.; Sheta, A.F.A.; Alkanhal, M.A. A compact dual circular patch pattern reconfigurable antenna. *Microw. Opt. Technol. Lett.* **2018**, *60*, 2762–2768. [\[CrossRef\]](#)
13. Lee, J.N.; Kim, J.H.; Park, J.K.; Kim, J.S. Design of dual-band antenna with U-shaped open stub for WLAN/UWB applications. *Microw. Opt. Technol. Lett.* **2009**, *51*, 284–289. [\[CrossRef\]](#)
14. Park, S.Y.; Park, J.K.; Kim, J.S. Dual-band antenna design using M-shaped open stub. *Microw. Opt. Technol. Lett.* **2011**, *53*, 455–458. [\[CrossRef\]](#)
15. Wang, L.; Chen, J.; Ping, Y.; Han, L.; Zhang, W. Design of a Dual-band Monopole Antenna for WLAN Applications. In Proceedings of the 2019 Computing, Communications and IoT Applications (ComComAp), Shenzhen, China, 26–28 October 2019; pp. 167–169.
16. Eltresy, N.; Elsheakh, D.N.; Abdallah, E.A.; Elhennawy, H.M. Multi band dual linearly polarized 2×2 antenna array for powering sensors in IoT systems. In Proceedings of the IEEE Global Conference on Internet of Things (GCIoT), Alexandria, Egypt, 5–7 December 2018; pp. 5–7.
17. Romputtal, A.; Phongcharoenpanich, C. IoT-Linked Integrated NFC and Dual Band UHF/2.45 GHz RFID Reader Antenna Scheme. *IEEE Access* **2019**, *7*, 177832–177843. [\[CrossRef\]](#)

18. Darimireddy, N.K.; Reddy, R.R.; Prasad, A.M. Asymmetric and symmetric modified bow-tie slotted circular patch antennas for circular polarization. *ETRI J.* **2018**, *40*, 561–569. [\[CrossRef\]](#)
19. Chen, Y.-Y.; Jiao, Y.-C.; Zhao, G.; Zhang, F.; Liao, Z.-L.; Tian, Y. Dual-Band Dual-Sense Circularly Polarized Slot Antenna With a C-Shaped Grounded Strip. *IEEE Antennas Wirel. Propag. Lett.* **2011**, *10*, 915–918. [\[CrossRef\]](#)
20. Wang, Z.; Zhang, G.-X.; Yin, Y.; Wu, J. Design of a Dual-Band High-Gain Antenna Array for WLAN and WiMAX Base Station. *IEEE Antennas Wirel. Propag. Lett.* **2014**, *13*, 1721–1724. [\[CrossRef\]](#)
21. Li, Y.; Zhao, Z.; Tang, Z.; Yin, Y. Differentially Fed, Dual-Band Dual-Polarized Filtering Antenna with High Selectivity for 5G Sub-6 GHz Base Station Applications. *IEEE Trans. Antennas Propag.* **2020**, *68*, 3231–3236. [\[CrossRef\]](#)
22. Darimireddy, N.K.; Reddy, R.R.; Prasad, A.M. Asymmetric triangular semi-elliptic Slotted Patch antennas for wireless applications. *Radioengineering* **2018**, *27*, 85. [\[CrossRef\]](#)
23. Wang, H.; Liu, S.-F.; Zhang, L.; Li, P.; Chen, L.; Shi, X.-W. Compact wideband and dual-band antenna with directional patterns. *Microw. Opt. Technol. Lett.* **2015**, *57*, 2742–2745. [\[CrossRef\]](#)
24. Li, L.; Zhang, X.; Yin, X.; Zhou, L. A Compact Triple-Band Printed Monopole Antenna for WLAN/WiMAX Applications. *IEEE Antennas Wirel. Propag. Lett.* **2016**, *15*, 1853–1855. [\[CrossRef\]](#)
25. Chen, W.-S.; Yang, C.-K.; Lin, G.-Q. Compact design of printed antenna with a ground slot for USB applications. In Proceedings of the 2016 IEEE 5th Asia-Pacific Conference on Antennas and Propagation (APCAP), Kaohsiung, Taiwan, 26–29 July 2016; pp. 127–128. [\[CrossRef\]](#)
26. Saxena, S.; Kanaujia, B.K.; Dwari, S.; Kumar, S.; Tiwari, R. A compact microstrip fed dual polarised multiband antenna for IEEE 802.11 a/b/g/n/ac/ax applications. *AEU Int. J. Electron. Commun.* **2017**, *72*, 95–103. [\[CrossRef\]](#)
27. Tan, M.-T.; Wang, B.-Z. A Compact Dual-Band Dual-Polarized Loop-Slot Planar Antenna. *IEEE Antennas Wirel. Propag. Lett.* **2015**, *14*, 1742–1745. [\[CrossRef\]](#)
28. Zhuo, L.; Han, H.; Shen, X.; Zhao, H. A U-shaped wide-slot dual-band broadband NB-IoT antenna with a rectangular tuning stub. In Proceedings of the 2020 IEEE 4th Information Technology, Networking, Electronic and Automation Control Conference (ITNEC), Chongqing, China, 12–14 June 2020; Volume 1, pp. 123–128.
29. Sheta, A.; Dib, N.; Mohra, A. Investigation of new nondegenerate dual-mode microstrip patch filter. *IEE Proc. Microw. Antennas Propag.* **2006**, *153*, 89–95. [\[CrossRef\]](#)
30. Alkanhal, M.; Sheta, A.F. A novel dual-band reconfigurable square-ring microstrip antenna. *Prog. Electromagn. Res.* **2007**, *70*, 337–349. [\[CrossRef\]](#)
31. Sheta, A.F. A small size dual-mode patch filter. *Int. J. Appl. Electromagn. Mech.* **2008**, *28*, 117–122. [\[CrossRef\]](#)
32. Sheta, A.F.; Al-Eshaikh, M.A. A New Small Size Non-degenerate Dual-mode Patch Filter. *J. Electromagn. Waves Appl.* **2011**, *25*, 1504–1514. [\[CrossRef\]](#)
33. Al-Yasir, Y.I.A.; Alkafaji, M.K.; Alhamadani, H.A.; Parchin, N.O.; Elfergani, I.; Saleh, A.L.; Rodriguez, J.; Abd-Alhameed, R.A. A New and Compact Wide-Band Microstrip Filter-Antenna Design for 2.4 GHz ISM Band and 4G Applications. *Electronics* **2020**, *9*, 1084. [\[CrossRef\]](#)
34. Islam, M.S.; Ullah, A.; Beng, G.K.; Amin, N.; Misran, N. A Modified Meander Line Microstrip Patch Antenna with Enhanced Bandwidth for 2.4 GHz ISM-Band Internet of Things (IoT) Applications. *IEEE Access* **2019**, *7*, 127850–127861. [\[CrossRef\]](#)
35. Saghati, A.P.; Azarmanesh, M.; Zaker, R. A Novel Switchable Single- and Multifrequency Triple-Slot Antenna for 2.4-GHz Bluetooth, 3.5-GHz WiMax, and 5.8-GHz WLAN. *IEEE Antennas Wirel. Propag. Lett.* **2010**, *9*, 534–537. [\[CrossRef\]](#)
36. Kulkarni, J. Multi-band printed monopole antenna conforming bandwidth requirement of GSM/WLAN/WiMAX standards. *Prog. Electromagn. Res. Lett.* **2020**, *91*, 59–66. [\[CrossRef\]](#)
37. Mansour, R. Design of superconductive multiplexers using single-mode and dual-mode filters. *IEEE Trans. Microw. Theory Tech.* **1994**, *42*, 1411–1418. [\[CrossRef\]](#)
38. Du, Z.; Gong, K.; Fu, J.; Gao, B. Analysis of microstrip fractal patch antenna for multi-band communication [by FDTD]. *Electron. Lett.* **2001**, *37*, 805–806. [\[CrossRef\]](#)
39. Elrashidi, A.; Elleithy, K.; Bajwa, H. Performance Analysis of a Microstrip Printed Antenna Conformed on Cylindrical Body at Resonance Frequency 4.6GHz for TM01 Mode. *Procedia Comput. Sci.* **2012**, *10*, 775–784. [\[CrossRef\]](#)
40. Liu, N.-W.; Zhu, L.; Choi, W.-W.; Zhang, J.-D. A Novel Differential-Fed Patch Antenna on Stepped-Impedance Resonator with Enhanced Bandwidth under Dual-Resonance. *IEEE Trans. Antennas Propag.* **2016**, *64*, 4618–4625. [\[CrossRef\]](#)
41. Liu, N.-W.; Zhu, L.; Choi, W.-W. A Differential-Fed Microstrip Patch Antenna with Bandwidth Enhancement under Operation of TM10 and TM30 Modes. *IEEE Trans. Antennas Propag.* **2017**, *65*, 1607–1614. [\[CrossRef\]](#)
42. Wang, J.; Liu, Q.; Zhu, L. Bandwidth Enhancement of a Differential-Fed Equilateral Triangular Patch Antenna via Loading of Shorting Posts. *IEEE Trans. Antennas Propag.* **2016**, *65*, 36–43. [\[CrossRef\]](#)
43. Parizi, S.A.R. Bandwidth Enhancement Techniques. In *Trends in Research on Microstrip Antennas*; IntechOpen: London, UK, 2017; Volume 1.
44. Kumar, A.; Gupta, N.; Gautam, P.C. Gain and Bandwidth Enhancement Techniques in Microstrip Patch Antennas—A Review. *Int. J. Comput. Appl.* **2016**, *148*, 9–14. [\[CrossRef\]](#)
45. Elsaygher, R.M. Study on bandwidth enhancement techniques of microstrip antenna. *J. Electr. Syst. Inf. Technol.* **2016**, *3*, 527–531. [\[CrossRef\]](#)
46. Waterhouse, R. *Microstrip Patch Antennas: A Designer's Guide*; Springer Science & Business Media: New York, NY, USA, 2003.

47. Kumar, G.; Ray, K.P. *Broadband Microstrip Antennas*; Artech House: London, UK, 2003.
48. Kushwaha, R.K.; Karuppanan, P. Proximity-coupled high gain graphene patch antenna using holey dielectric superstrate for terahertz applications. *Optik* **2021**, *240*, 166793. [[CrossRef](#)]
49. Swetha, R.; Anjaneyulu, L. Novel Design and Characterization of Wide Band Hook Shaped Aperture Coupled Circularly Polarized Antenna for 5G Application. *Prog. Electromagn. Res. C* **2021**, *113*, 161–175. [[CrossRef](#)]
50. Rosado-Sanz, J.; Jarabo-Amores, M.; Mata-Moya, D.; Gómez-Del-Hoyo, P.; Del-Rey-Maestre, N. Broadband modified-circle-shape patch antenna with H-aperture feeding for a passive radar array. *Aerosp. Sci. Technol.* **2021**, *110*, 106445. [[CrossRef](#)]
51. Sun, J.; Luk, K.-M. A Circularly Polarized Water Patch Antenna. *IEEE Antennas Wirel. Propag. Lett.* **2020**, *19*, 926–929. [[CrossRef](#)]
52. Lin, W.; Wong, H. Wideband Circular-Polarization Reconfigurable Antenna with L-Shaped Feeding Probes. *IEEE Antennas Wirel. Propag. Lett.* **2017**, *16*, 2114–2117. [[CrossRef](#)]
53. Sumithra, P.; Kannadassan, D. Bandwidth Enhancement of Low-Profile Slot Antennas using Theory of Characteristic Modes. *AEU Int. J. Electron. Commun.* **2021**, *138*, 153868. [[CrossRef](#)]
54. Moussa, K.; Amar, A.; Mabrouk, M.; Mohamed, H. Slotted E-Shaped Meta-Material Decoupling Slab for Densely Packed MIMO Antenna Arrays. *Micromachines* **2021**, *12*, 873. [[CrossRef](#)]
55. Mistry, K.K.; Lazaridis, P.I.; Zaharis, Z.D.; Loh, T.H. Design and Optimization of Compact Printed Log-Periodic Dipole Array Antennas with Extended Low-Frequency Response. *Electronics* **2021**, *10*, 2044. [[CrossRef](#)]
56. Gatti, R.V.; Rossi, R.; Dionigi, M. Single-Layer Line-Fed Broadband Microstrip Patch Antenna on Thin Substrates. *Electronics* **2020**, *10*, 37. [[CrossRef](#)]
57. Tran, H.H.; Bui, C.D.; Nguyen-Trong, N.; Nguyen, T.K. A Wideband Non-Uniform Metasurface-Based Circularly Polarized Reconfigurable Antenna. *IEEE Access* **2021**, *9*, 42325–42332. [[CrossRef](#)]
58. Elahi, M.; Trinh-Van, S.; Yang, Y.; Lee, K.-Y.; Hwang, K.-C. Compact and High Gain 4×4 Circularly Polarized Microstrip Patch Antenna Array for Next Generation Small Satellite. *Appl. Sci.* **2021**, *11*, 8869. [[CrossRef](#)]
59. Wang, J.; Cui, W.; Zhou, Y.; Liu, R.; Wang, M.; Fan, C.; Zheng, H.; Li, E. Design of Wideband Antenna Array with Dielectric Lens and Defected Ground Structure. *Electronics* **2021**, *10*, 2066. [[CrossRef](#)]
60. Peng, H.; Zhi, R.; Yang, Q.; Cai, J.; Wan, Y.; Liu, G. Design of a MIMO Antenna with High Gain and Enhanced Isolation for WLAN Applications. *Electronics* **2021**, *10*, 1659. [[CrossRef](#)]
61. Geozondas. Time-Domain Antenna Measurement Systems. Available online: https://geozondas.com/main_page.php?pusl=12 (accessed on 10 October 2021).